Revealing the correlation between asymmetric structure and low thermal conductivity in Janus-graphene via machine learning force constant potential

View Online   Export Citation   CrossMark

Linfeng Yu,[1] (ID) Kexin Dong,[1] Qi Yang,[1] Yi Zhang,[1] Xiong Zheng,[1] Huimin Wang,[2] (ID) Zhenzhen Qin,[3] (ID) and Guangzhao Qin[1,4,5,a] (ID)

AFFILIATIONS

[1]State Key Laboratory of Advanced Design and Manufacturing Technology for Vehicle, College of Mechanical and Vehicle Engineering, Hunan University, Changsha 410082, People's Republic of China
[2]Hunan Key Laboratory for Micro-Nano Energy Materials & Device and School of Physics and Optoelectronics, Xiangtan University, Xiangtan 411105, Hunan, China
[3]School of Physics and Microelectronics, Zhengzhou University, Zhengzhou 450001, China
[4]Research Institute of Hunan University in Chongqing, Chongqing 401133, China
[5]Greater Bay Area Institute for Innovation, Hunan University, Guangzhou 511300, Guangdong Province, China

[a]Author to whom all correspondence should be addressed: gzqin@hnu.edu.cn

ABSTRACT

Understanding the fundamental link between structure and functionalization is crucial for designing and optimizing functional materials, since different structural configurations could trigger materials to demonstrate diverse physical and chemical properties. However, the correlation between crystal structure and thermal conductivity (κ) remains unclear. In this study, taking two-dimensional (2D) carbon allotropes Janus-graphene and graphene as study cases, we utilize phonon Boltzmann transport equation combined with machine learning potential to thoroughly investigate the complex folding structure of pure sp^2 hybridized Janus-graphene from the perspective of crystal structure, phonon modal resolved thermal transport, and atomic interactions, with the goal of identifying the underlying relationship between 2D geometry and κ. The results reveal that the folded structure in Janus-graphene causes strong symmetry breaking, significantly reduces phonon group velocities, increases phonon–phonon scattering, and ultimately leads to low κ. These findings enhance our understanding of how atomic structure folding affects thermal transport and the relationship between structure and functionalization.

Published under an exclusive license by AIP Publishing. https://doi.org/10.1063/5.0237434

The phonon behavior in two-dimensional (2D) materials is influenced by structural confinement and dimensionality effects, which differ from those observed in conventional three-dimensional (3D) materials. In 2D materials, layered structure restricts atomic coupling to the *in-plane* direction, leading to heat conduction primarily through *in-plane* phonon transport.[1,2] The diversity and complexity of atomic bonding types and dimensional effects make accurate estimations and general interpretations for the thermal conductivity (κ) of the numerous carbon allotropes more challenging, but they also inspire strong research interest. For instance, Choudhry *et al.*[21] investigated the thermal transport properties of solely sp^2 hybridized 2D carbon planar structures and discovered that the poor κ is caused by the

superstructure's acoustic mode folding effect. Our previous study[4] revealed that the insertion of the sp^3 hybrid structure can further induce substantial phonon–phonon scattering, affecting the thermal transport properties. Interestingly, Giri *et al.*[5] discovered that in amorphous carbon materials, increasing the amount of sp^3 hybridization may greatly boost the contribution of propagating modes, resulting in a fourfold increase in κ, which contrasts to its role in 2D carbon materials. While sp^3 hybridized carbon atoms contribute an extra scattering mechanism that might boost the contribution of propagating modes and hence increase κ, amorphous carbon materials have carbon atoms organized chaotically. It also reveals that the interaction between the specific material structure and the pure sp^2 (or sp^3) hybrid structure

affecting the heat transfer capability is complex, leading to the fact that the performance of κ is affected by various architectures and bond hybridizations. Moreover, the notable features of 2D carbon structures include not only *in-plane* structural folding but also *out-of-plane* morphological expansion, leaving a major gap in our understanding of the link between the shape of these structures and κ.

However, despite the rich and complex carbon structures enabling diverse phonon transport behaviors, the precise κ remains elusive. Complex and asymmetric configurations require computational resources to perform high-order partial derivatives of potential energy, especially the fourth-order and above interatomic force constants, leading to high costs for obtaining thermal transport properties, while solving the phonon Boltzmann transport equation (BTE) with first-principles calculations. As for the molecular dynamics method, it can consider higher-order phonon effects and may exhibit higher efficiencies, such as the four-phonons in c-BAs,[6] and it relies heavily on the precise interatomic potential function. The separation of various orders of phonon–phonon scattering is difficult. Hence, obtaining κ for complex carbon configurations is often difficult due to the high computational cost of higher-order force constants and the limited availability of interatomic potential functions. Although substantial progress has been achieved in understanding the κ of 2D carbon

structures,[3–5,7–10] it is necessary to investigate the mechanism of different structural morphologies on κ to gain a more comprehensive understanding of the phonon propagation and scattering behavior in 2D carbon structures by more accessible methods.

In this study, we exploit the phonon BTE combined with machine learning potential to investigate pure sp^2 hybrid carbon materials Janus-graphene[11] and graphene with complex folded structures. Compared with traditional first-principles and molecular dynamics methods, machine learning force constant potential methods can efficiently evaluate higher-order phonon effects and can quickly obtain potential energy surfaces and their partial derivatives without significantly increasing computing resources for asymmetric complex lattices. In this manner, we focus on the crystal structure, phonon properties, phonon–phonon scattering, and atomic interaction levels of 2D carbon materials Janus-graphene and graphene, with the goal to establish a link between asymmetric geometry and thermal transport properties in the Janus-graphene.

We used a linear programming-based machine-learning interatomic potential (MLIP) developed by Shapeev *et al.*[12] Using the provided potential function model file (*20.mtp*) as a reference, we set the minimum and maximum radial distances $min\_dist = 1.27$ Å and $max\_dist = 6$ Å. Figure 1(a) shows the top view and side view of the
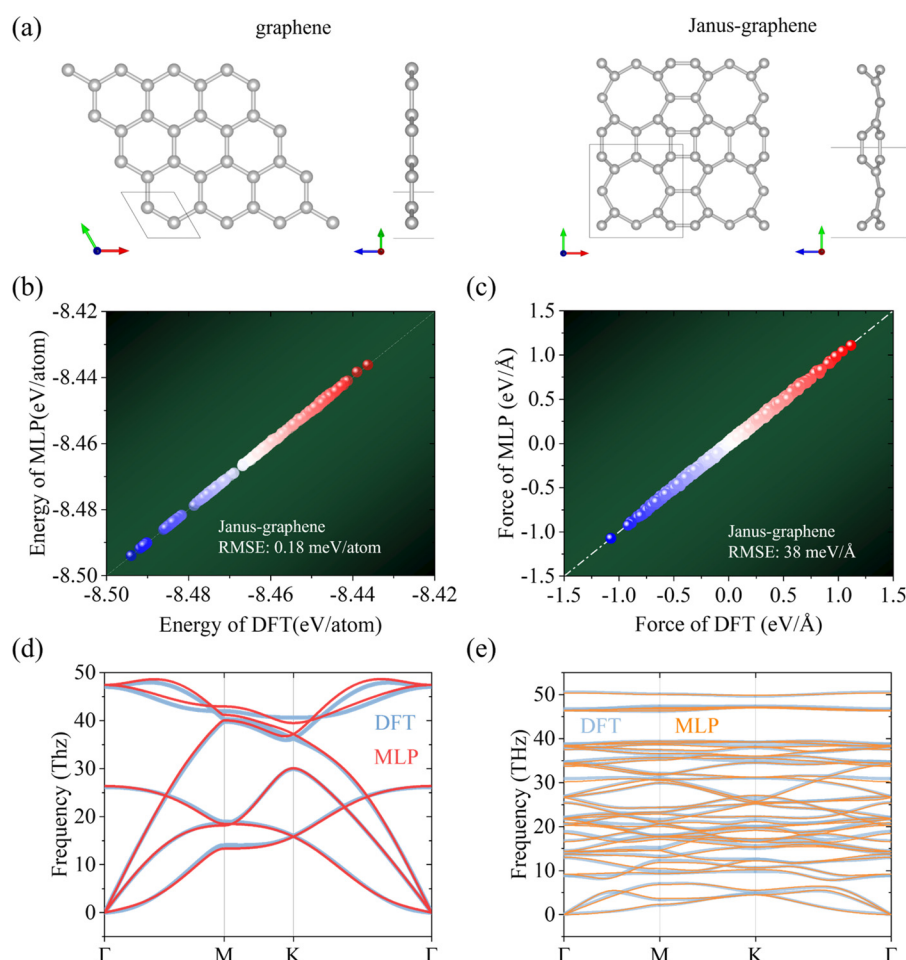

FIG. 1. Machine learning force constant potentials and density functional theory (DFT) calculations. (a) Crystal structures for graphene and Janus-graphene. (b) Energy and (c) force of Janus-graphene. Phonon dispersion in (d) graphene and (e) Janus-graphene.

graphene and Janus-graphene crystal structures. The structures and corresponding energies and forces at different temperatures are calculated by *ab initio* molecular dynamics (AIMD), which are used to construct the datasets required for the simulations. (More calculation details can be found in supplementary material, Note. S1.) Unlike the molecular dynamics potential, the main purpose of the interatomic force constant potential is to compute the low-order and high-order derivatives of energy based on the finite displacement method to solve the phonon Boltzmann transport equation (BTE), indicating a larger significance for the energy and force of static small displacements. As shown in Figs. 1(b) and 1(c), the energies and forces predicted by the machine-learned potential (MLP) were compared with the results from first-principles calculations, where good agreement with each other demonstrated the potential function model's strong fitting ability for predicting the energy and force for the perturbed configuration of Janus-graphene. The low root mean square error *RMSE* $= \sqrt{\frac{1}{N}\sum_{i=1}^{N}\left(x_{MLP,i} - y_{DFT,i}\right)^2}$ [where $x_{MLP,i}$ denotes the predicted energy values from the machine learning model, while $y_{DFT,i}$ indicates the corresponding actual energy values obtained from density functional theory (DFT)] of energies (RMSE: 0.18 meV) and forces (RMSE

38 meV/A) indicates the high quality and strong robustness of the machine learning potential function model. In solving BTE, machine learning networks can map the energies and forces produced by AIMD to obtain low-order and high-order force constants. The third- and fourth-order force constants among them are often enough to describe their anharmonicity. Therefore, we focus primarily on evaluating the role of three-phonon and four-phonon interactions, with particular emphasis on the former.

To validate the accuracy of the machine learning potential function model, we first constructed the phonon dispersion and compared it to density functional theory (DFT) results. The influence of different supercells on phonon dispersion was tested in Janus-graphene, and the $4 \times 4 \times 1$ supercell was finally selected as shown in supplementary material, Fig. S1. The results obtained by the MLP model are in good agreement with those computed using DFT, as shown in Figs. 1(d) and 1(e). Unlike graphene, Janus-graphene exhibits more phonon branches, resulting in additional phonon modes due to the asymmetry in its inherent structure. The acoustic phonon branch is significantly suppressed, demonstrating strong phonon softening. Consequently, this leads to a significantly weakened contribution of the acoustic phonon branch that dominates κ, contributing to an ultralow κ, as explained later.
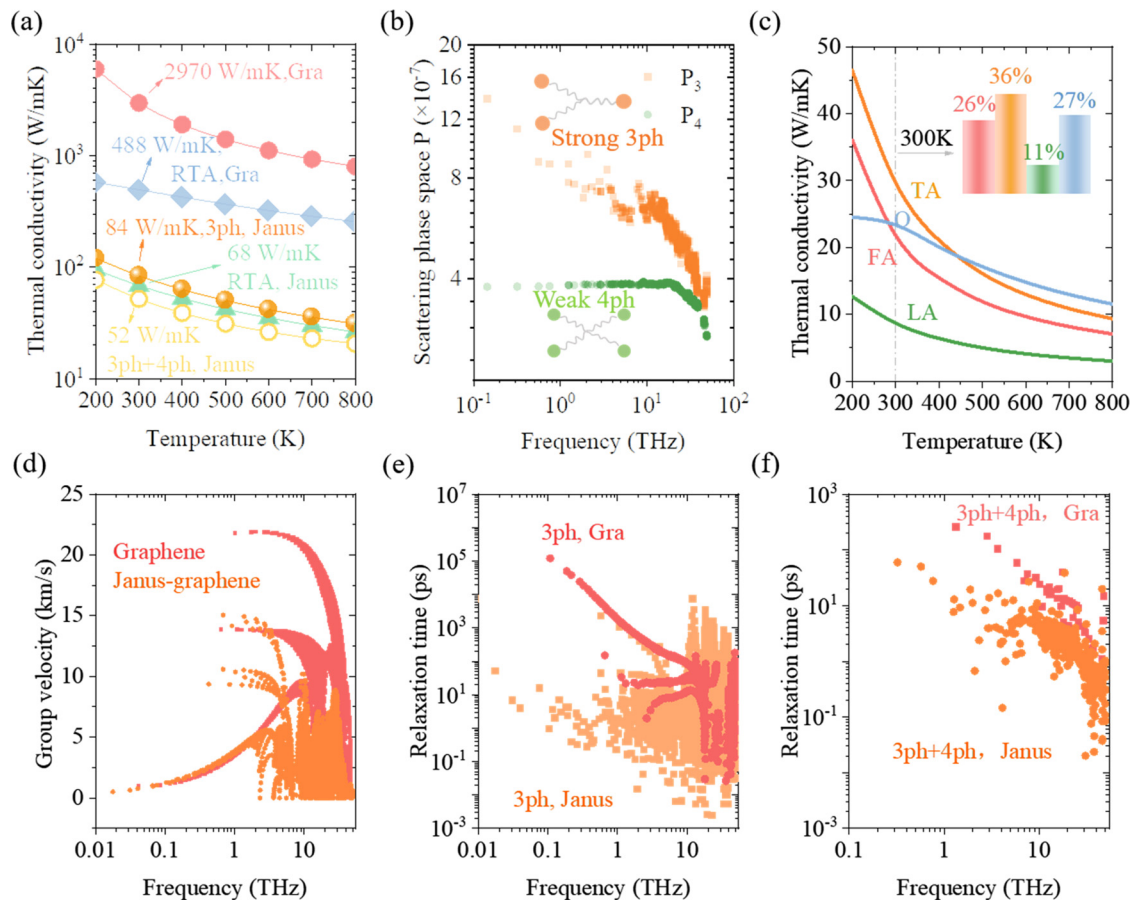

FIG. 2. Thermal transport properties. (a) Temperature dependent thermal conductivity in graphene and Janus-graphene. (b) Three- and four-phonon scattering in phase space. (c) Temperature-dependent thermal conductivity contribution for different branches. Mode-level (d) group velocities and relaxation times for (e) three phonons and (f) four phonons.

In semiconductors, phonons are the main carriers of heat, while electrons serve as the primary carriers in metals. Although graphene exhibits semi-metallic properties, its electronic contribution to thermal conductivity is significantly lower than that of phonons.[1,13,14] In contrast, Janus-graphene has a wide bandgap of 2.01 eV, as illustrated in supplementary material, Fig. S2. Thus, phonons play a dominant role in the thermal conductivity of both graphene and Janus-graphene, and this study still focuses on analyzing the influence of phonons. As shown in Fig. 2(a), the temperature-dependent behavior of graphene and Janus-graphene was determined using the iterative (ITE) and relaxation time approximation (RTA) methods. Based on the ITE approach, κ at 300 K for Janus-graphene and graphene is 84 and 2790 W/mK, respectively, which are in good agreement with the DFT results as shown in supplementary material, Fig. S3. In addition, we also compare the robustness of the force constants for graphene as shown in supplementary material, Note S2, where the robust force constants from the MLP agree well with the DFT results. More information about the phonon BTE can be found in supplementary material, Note S3. These results demonstrate the accuracy and robustness of machine learning-driven force constant potentials. Note that κ of Janus-graphene is almost two orders of magnitude lower than that of graphene due to the double symmetry breaking caused by *in-plane* and *out-of-plane* superfolding.

Building on the study of Mortazavi[15] and Han et al.,[16] we reformulated the four-phonon interface (*Fourthorder_MTP.py*) between the machine learning potential and the phonon BTE solver. As shown in supplementary material, Fig. S4, the two can be well matched and

are consistent with the previous results of Feng et al.,[17] revealing a high-precision description of higher-order force constants by the machine learning model. In addition, the mode-level group velocity and relaxation time considering three-phonon and four-phonon mechanisms for graphene are compared in supplementary material, Fig. S5, where the results of the MLP method and the DFT method are in good agreement. The role of four phonons may be significant at high temperatures or in some special cases, such as flat bands in AgCrSe$_2$[18] or huge acoustic-optical band gaps in c-BAs.[19–23] Our MLP method ($\sim$900 W/mK) is consistent with previous results by Feng et al.[17] However, κ after considering the four-phonon scattering in Janus-graphene is 52 W/mK, but this is not a substantial order of magnitude reduction, indicating that the three-phonon scattering still plays a dominant role in the phonon–phonon scattering process. In Janus-graphene, the three-phonon scattering phase space (P_3) significantly exceeds that of the four-phonon (P_4), indicating that the four-phonon scattering is weaker.

The contribution of different phonon branches for Janus-graphene to κ is shown in Fig. 2(c). Since phonons follow the Bose–Einstein distribution, the contributions of all phonon branches decrease with increasing temperature in the temperature range of 200–800 K. κ of Janus-graphene at 300 K is mostly provided by the FA, TA, and optical branches. The TA branch has contributed most, reaching 36%, which is substantially higher than graphene. At 300 K, the contribution percentage of FA branch in graphene approaches 80%, nearly fully governing κ, but the FA branch in Janus-graphene occupies just 26%, a considerably fewer proportion than in graphene. Although after
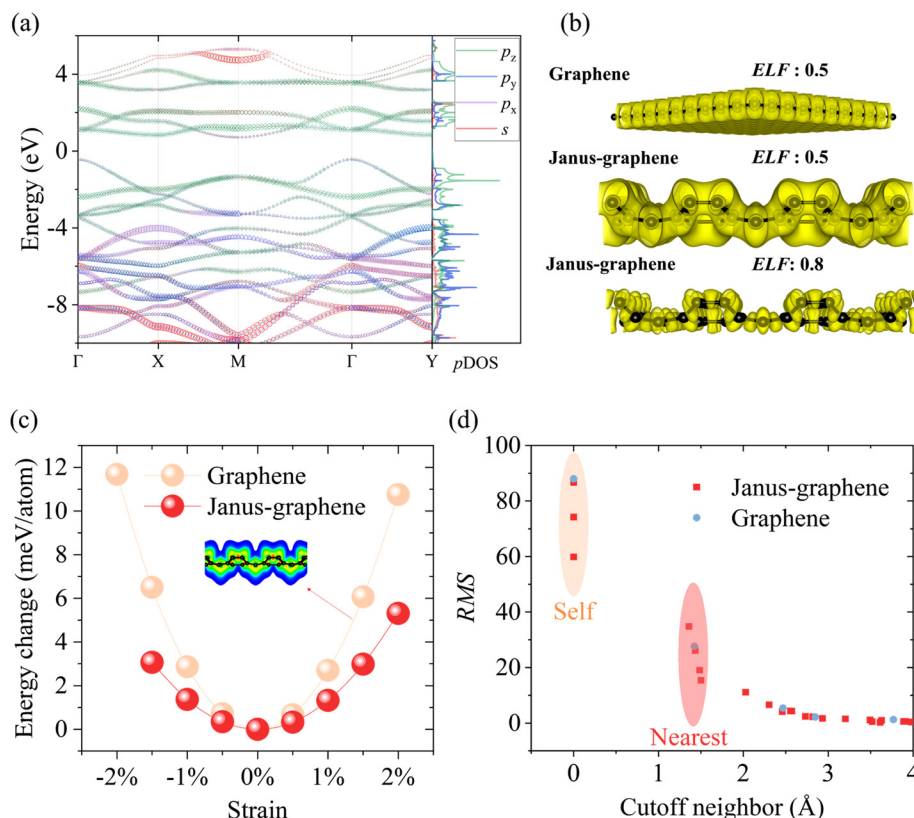

FIG. 3. Electronic properties and lattice anharmonicity. (a) Orbital hybridization of Janus-graphene. (b) 3D dimensionless electron localization function comparison of graphene and Janus-graphene. (c) Comparison of atomic vibration potential wells of graphene and Janus-graphene. (d) Comparison of atomic vibration RMS displacement of graphene and Janus-graphene. Embedded are the averaged self-interactions and nearest-neighbor interactions.

considering four phonons, the contribution of FA phonons in graphene can still be as high as 75%,[24] suggesting that the Janus configuration significantly weakens the contribution of the FA branch, leading to a decrease in κ. Furthermore, from the mode-level phonon properties, the low thermal conductivity can be traced back to the low group velocity [Fig. 2(d)], relaxation time [Figs. 2(e) and 2(f)], and strong anharmonicity. The relatively large Grüneisen parameters in Janus-graphene can be found in supplementary material, Fig. S6, which quantifies the anharmonicity.

In graphene, two carbon atoms form a strong and stable covalent bond in pure sp^2 hybridization by sharing electron pairs. In sp^2 hybridization, one $2s$ orbital and two $2p$ (p_x and p_y) orbitals of carbon atoms are linearly combined to form three equivalent sp^2 hybridization orbitals. These sp^2 hybrid orbitals form three σ bonds in graphene, which lie in a plane and are separated by an angle of $120°$ from each other. The remaining one p_z orbital is perpendicular to the plane and forms a π bond, responsible for the π electron conjugated system in graphene. This ideal electronic configuration exhibits strong symmetry, which limits the anharmonicity in the atomic vibration process due to the perfectly planar structure.[25,26]

In contrast, the *out-of-plane* buckling significantly destroys the planar features, especially the p_z orbitals of Dirac cones (for graphene), making the p_z electrons localized in the *out-of-plane* direction to form a quasi-sp^3 hybridization as shown in Fig. 3(a), i.e., dangling bond.[27,28] The dangling bond states in Janus-graphene are activated, showing strong stereochemical activity. As shown in Fig. 3(b), the electron localization function (ELF) potential energy surface can further show the local morphology of their electron distribution, where strong spatial distribution asymmetry is exhibited in Janus-graphene.

During thermal vibrations, the uniformly distributed ELF in graphene results in weak anharmonic interactions in wavefunction overlap due to strong symmetries. In contrast, the pronounced asymmetry in the Janus-graphene induces strong nonlinear Coulomb forces due to *out-of-plane* buckling superfolding, leading to its strong anharmonicity. Strong anharmonicity enables further insight into be gained through the anharmonic potential well shown in Fig. 3(c), where Janus-graphene exhibits a wider potential energy surface at the same amplitude, indicating that atoms need more energy to recover during vibration. As shown in Fig. 3(d), the force constant root mean square (RMS) distribution of Janus-graphene is more inhomogeneous
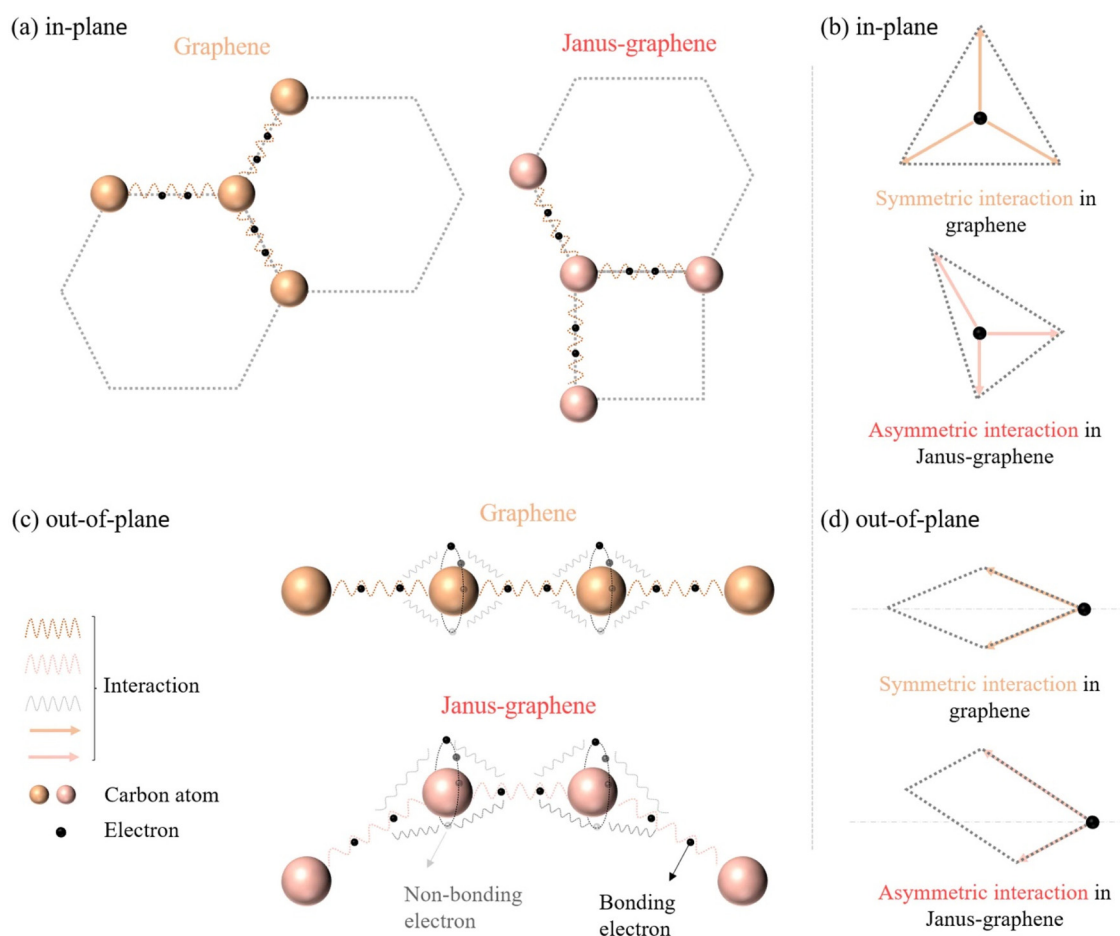

FIG. 4. Folded structure-induced asymmetric atomic interactions. Schematic diagram of (a) atomic structure and (b) atomic interactions along the *in-plane* direction. Schematic diagram of (c) atomic structure and (d) atomic interactions along the *out-of-plane* direction.

23 November 2024 10:50:13

compared to that of graphene, indicating non-uniform atomic repulsion in wave function overlap. This inhomogeneity of RMS originates from the inhomogeneity of the force constant, leading to the renormalized phonon–phonon scattering, which finally leads to a significant decrease in the κ of Janus-graphene.

Ultimately, broad conclusions about the uneven distribution of force constants can be drawn from the folding evolution of atomic geometries. As shown in Figs. 4(a) and 4(b), carbon atoms form a perfect hexagon in planar graphene, with bond angles of 120° due to sp^2 hybridization. This hexagonal arrangement creates a honeycomb lattice with high symmetry. Consequently, the nonlinear Coulomb repulsion of electrons in graphene is minimized during thermal vibrations. In other words, *out-of-plane* phonon–phonon scattering is governed by a symmetry in which the odd number of FA phonons involved is mapped onto themselves and prohibited by the phonon selection rule.

However, when the pure 6-membered ring is transformed into a 4–6–8 ring, the bond angle deviates from the ideal 120° in the *in-plane* direction. For biphenylene and Y-biphenylene [Fig. S7(a)], the *in-plane* bond angles are approximately 90°, 120°, and 180°, leading to the breaking of the central rotational and translational symmetry and thus the redistribution of the Coulomb repulsion between the in-plane charges. Among them, phonon–phonon scattering channels previously suppressed by symmetry are activated.

As shown in Figs. 4(c) and 4(d), when the *out-of-plane* configuration is introduced, the Coulomb repulsion along the *out-of-plane* direction is renormalized, resulting in a further broken symmetry and a decrease in κ. Therefore, κ of Janus-graphene is not only lower than that of graphene, but also about an order of magnitude lower than that of biphenylene and Y-biphenylene [Fig. S7(b)]. Due to the same elements and similar bond lengths, the diversity spatial distribution (main bond angles) induces various types of *in-plane* and *out-of-plane* Coulomb repulsion redistributions, resulting in enhanced asymmetry and reduced thermal conductivity, as shown in Fig. 4.

Thus, a insight can be broadly applied to explain the thermal transport properties in other 2D carbon allotropes, such as D-graphene, T-graphene, and kagome-graphene.[3,8,29] The potential mapping link between atomic-scale geometry and phonon level can also serve as a design foundation for thermally functional materials, as well as valuable clues for the prediction and regulation of thermal transport properties of abundant 2D carbon allotropes or carbon-based phononic crystals.

In summary, we take advantage of the powerful fitting ability of machine learning methods to solve the phonon BTE by establishing a regression potential energy surface from DFT to MLP, thereby obtaining the thermal transport properties of Janus-graphene and graphene. Most importantly, we explored the mechanism of the evolution of thermal transport properties with structure in Janus-graphene: in-plane and out-of-plane fold evolution, which can suppress the contribution of flexible acoustic (FA) phonons, resulting in low group velocity, weak phonon–phonon scattering, and strong asymmetry, which finally contributes to low κ.

See the supplementary material for the following: Note S1: additional calculation details; Note S2: robustness assessment of force constant potential driven by machine learning; Note S3: calculation details for phonon Boltzmann transport equation; Fig. S1: phonon dispersion test; Fig. S2: energy band of Janus-graphene based on HSE06 functional; Fig. S3; comparison of thermal conductivity for graphene calculated by machine learning model and density functional theory; Fig. S4: comparison of machine learning potentials and density functional theory models for the four-phonon effect in graphene; Fig. S5: comparison of phonon properties calculated by machine learning potentials and density functional theory calculations; Fig. S6: Grüneisen parameter for graphene and Janus-graphene; and Fig. S7: evolution trends of structure and thermal conductivity.

AUTHOR DECLARATIONS
Conflict of Interest

The authors have no conflicts to disclose.

Author Contributions

Linfeng Yu: Conceptualization (equal); Writing – original draft (equal); Writing – review & editing (equal). **Kexin Dong:** Writing – review & editing (equal). **Qi Yang:** Writing – review & editing (equal). **Yi Zhang:** Writing – review & editing (equal). **Xiong Zheng:** Writing – review & editing (equal). **Huimin Wang:** Writing – review & editing (equal). **Zhenzhen Qin:** Writing – review & editing (equal). **Guangzhao Qin:** Writing – review & editing (equal).

DATA AVAILABILITY

The data that support the findings of this study are available from the corresponding author upon reasonable request.

REFERENCES

[1]S. Chen, Q. Wu, C. Mishra, A. A. Balandin, R. S. Ruoff *et al.*, "Thermal conductivity of isotopically modified graphene," Nat. Mater. **11**(3), 203–207 (2012).

[2]L. Lindsay, D. A. Broido, and N. Mingo, "Flexural phonons and thermal transport in graphene," Phys. Rev. B **82**(11), 115427 (2010).

[3]U. Choudhry, S. Yue, and B. Liao, "Origins of significant reduction of lattice thermal conductivity in graphene allotropes," Phys. Rev. B **100**(16), 165401 (2019).

[4]L. Yu, A. Chen, X. Wang *et al.*, "Softened $sp^2 - sp^3$ bonding network leads to strong anharmonicity and weak hydrodynamics in graphene+," Phys. Rev. B **106**(12), 125410 (2022).

[5]A. Giri, C. J. Dionne, and P. E. Hopkins, "Atomic coordination dictates vibrational characteristics and thermal conductivity in amorphous carbon," npj Comput. Mater. **8**(1), 1–7 (2022).

[6]Y. Ouyang, C. Yu, J. He *et al.*, "Accurate description of high-order phonon anharmonicity and lattice thermal conductivity from molecular dynamics simulations with machine learning potential," Phys. Rev. B **105**(11), 115202 (2022).

[7]M. Raeisi, B. Mortazavi, E. V. Podryabinkin *et al.*, "High thermal conductivity in semiconducting Janus and non-Janus diamanes," Carbon **167**, 51–61 (2020).

[8]H. Dong, Z. Zhang, Z. Feng *et al.*, "Origins of low lattice thermal conductivity in 2D carbon allotropes," J. Mater. Res. Technol. **11**, 1982–1990 (2021).

[9]F. Q. Wang, J. Yu, Q. Wang *et al.*, "Lattice thermal conductivity of penta-graphene," Carbon **105**, 424–429 (2016).

[10]H. P. Veeravenkata and A. Jain, "Density functional theory driven phononic thermal conductivity prediction of biphenylene: A comparison with graphene," Carbon **183**, 893–898 (2021).

[11]L. Yu, J. Xu, C. Shen *et al.*, "Janus graphene: A two-dimensional half-auxetic carbon allotrope with a nonchemical Janus configuration," Phys. Rev. B **109**(12), L121402 (2024).

[12]I. S. Novikov, K. Gubaev, E. V. Podryabinkin *et al.*, "The MLIP package: Moment tensor potentials with MPI and active learning," Mach. Learn.: Sci. Technol. **2**(2), 025002 (2021).

[13]S. Yiğen, V. Tayari, J. O. Island *et al.*, "Electronic thermal conductivity measurements in intrinsic graphene," Phys. Rev. B **87**(24), 241411 (2013).

[14]T. Y. Kim, C.-H. Park, and N. Marzari, "The electronic thermal conductivity of graphene," Nano Lett. **16**(4), 2439–2443 (2016).

[15]B. Mortazavi, E. V. Podryabinkin, I. S. Novikov *et al.*, "Accelerating first-principles estimation of thermal conductivity by machine-learning interatomic potentials: A MTP/ShengBTE solution," Comput. Phys. Commun. **258**, 107583 (2021).

[16]Z. Han, X. Yang, W. Li *et al.*, "FourPhonon: An extension module to ShengBTE for computing four-phonon scattering rates and thermal conductivity," Comput. Phys. Commun. **270**, 108179 (2022).

[17]T. Feng and X. Ruan, "Four-phonon scattering reduces intrinsic thermal conductivity of graphene and the contributions from flexural phonons," Phys. Rev. B **97**(4), 045202 (2018).

[18]L. Xie, J. H. Feng, R. Li *et al.*, "First-principles study of anharmonic lattice dynamics in low thermal conductivity AgCrSe$_2$: Evidence for a large resonant four-phonon scattering," Phys. Rev. Lett. **125**(24), 245901 (2020).

[19]N. K. Ravichandran and D. Broido, "Phonon-phonon interactions in strongly bonded solids: Selection rules and higher-order processes," Phys. Rev. X **10**(2), 021063 (2020).

[20]L. Lindsay, D. A. Broido, and T. L. Reinecke, "First-principles determination of ultrahigh thermal conductivity of boron arsenide: A competitor for diamond?," Phys. Rev. Lett. **111**(2), 025901 (2013).

[21]S. Li, Q. Zheng, Y. Lv *et al.*, "High thermal conductivity in cubic boron arsenide crystals," Science **361**(6402), 579–581 (2018).

[22]S. Yue, F. Tian, X. Sui *et al.*, "High ambipolar mobility in cubic boron arsenide revealed by transient reflectivity microscopy," Science **377**(6604), 433–436 (2022).

[23]J. Shin, G. A. Gamage, Z. Ding *et al.*, "High ambipolar mobility in cubic boron arsenide," Science **377**(6604), 437–440 (2022).

[24]Z. Han and X. Ruan, "Thermal conductivity of monolayer graphene: Convergent and lower than diamond," Phys. Rev. B **108**(12), L121412 (2023).

[25]D.-H. Wei, E. Zhou, J.-Y. Xu *et al.*, "Insight into vertical piezoelectric characteristics regulated thermal transport in van der Waals two-dimensional materials," Rare Met. **43**, 770–779 (2024).

[26]L.-F. Yu, J.-Y. Xu, C. Shen *et al.*, "Realizing ultra-low thermal conductivity by strong synergy of asymmetric geometry and electronic structure in boron nitride and arsenide," Rare Met. **42**(1), 210–221 (2023).

[27]S. B. Zhang and S.-H. Wei, "Surface energy and the common dangling bond rule for semiconductors," Phys. Rev. Lett. **92**(8), 086102 (2004).

[28]M. E. Turiansky, A. Alkauskas, L. C. Bassett *et al.*, "Dangling bonds in hexagonal boron nitride as single-photon emitters," Phys. Rev. Lett. **123**(12), 127401 (2019).

[29]P. Ying, T. Liang, Y. Du *et al.*, "Thermal transport in planar sp2-hybridized carbon allotropes: A comparative study of biphenylene network, pentaheptite and graphene," Int. J. Heat Mass Transfer **183**, 122060 (2022).

23 November 2024 10:50:13